# Chapter 10
# Fundamental Experiments and Quantum Technology Applications with Defect Centres in Diamond


**Oliver Benson**

**Abstract** The observation of single quantum objects has been a challenging task requiring advanced experimental techniques. With improved microscopy methodology it is nowadays possible to observe such objects in the solid state with compact setups even at room temperature. In this contribution we introduce defect centres in diamond and discuss two recent experiments. One concerns the direct observation of the quantum nature of light with not more but a single detector. The second one shows how to use defect centres as a valuable light source for quantum key distribution.

**Keywords** Diamond defect centre · Single photons · Light quantization · Superconducting detectors · Quantum key distribution · Quantum information

## 10.1 Introduction

Defect centers in diamond are stable atom-like objects, that emit light. This simple feature has nevertheless allowed for a large number of experiments and applications. The reason is that the very nature of light emitted from a single quantum system has quantum features as well. On the other hand, light, i.e. an electromagnetic field in the visible special range, is easy to detect, even at an ultra-low level of intensity. In this way the state of the emitter can be detected and even manipulated with light.

In this contribution we discuss two experiments with a defect centre in diamond, more precisely with a single nitrogen vacancy centre. Both experiments utilize the quantum nature of the emitted light. A first one is of fundamental nature [1], whereas a second one deals with an application in quantum information processing [2].

O. Benson (✉)
Nano-Optics, Institute of Physics, Humboldt-University, Berlin, Germany
e-mail: oliver.benson@physik.hu-berlin.de; https://www.physik.hu-berlin.de/de/nano



B. Di Bartolo et al. (eds.), *Quantum Nano-Photonics*, NATO Science for Peace and Security Series B: Physics and Biophysics,
https://doi.org/10.1007/978-94-024-1544-5_10

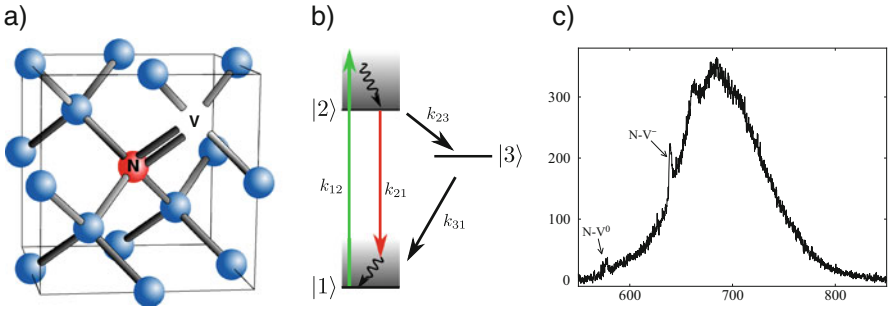


**Fig. 10.1** Nitrogen vacancy (NV) centre in diamond: (**a**) structure, (**b**) level scheme, (**c**) emission spectrum

## 10.2 Single Photon Emitters Based on Defect Centres in Diamond

Defect centres in diamond are the subject of intense research due to their exceptional role as single-photon sources at ambient condition [3]. Among the different defects, nitrogen vacancy (NV) centres are the best studied, a nitrogen replacing a carbon atom with an adjacent vacancy in the diamond lattice (Fig. 10.1a). A charged $NV^-$ and an uncharged $NV^0$ configuration of this defect could be identified, with zero phonon lines (ZPL) at 638 nm and 575 nm. At room temperature, single-photon emission around 700 nm with count rates up to $10^6$ counts/s can be observed from the $NV^-$. The spectrum of a single NV centre in a nanodiamond is shown in Fig. 10.1c. In nanodiamonds, we always observe both ZPLs attributed to (de-)charging effects. The optical transition occurs between two spin-triplet states ($|1\rangle \rightarrow |2\rangle$), but at least one singlet state is also present (Fig. 10.1b) and can be filled by intersystem crossing, which results in an additional bunching feature in the $g^{(2)}$-function. The presence of NV centres in nanodiamonds down to sizes of 5 nm make them superior fundamental building blocks in more complex, hybrid assembled photonic and plasmonic structures.

## 10.3 The Most Fundamental Experiment to Show the Quantum Nature of Light

### *10.3.1 Concept of the Experiment*

The first experiment based on an NV centre single photon source concerns non-classicality, i.e. a proof that light consists of photons. Many properties of a light emitter can be studied only by analysing auto-correlation functions of the electric field. Firstly, this holds for revealing the non-classical character of a quantum light

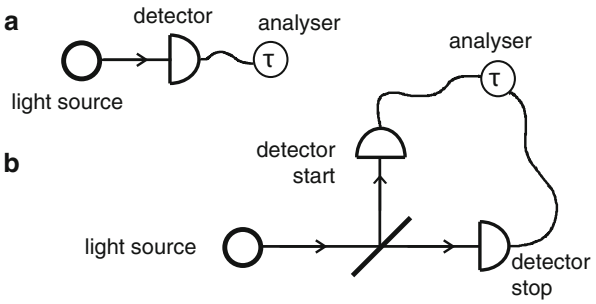


**Fig. 10.2** Scheme of setups to measure the second-order auto-correlation function of the electric field of a light source. (**a**) Measurement scheme with a single fast detector. (**b**) Conventional HBT-setup. (Reproduced from [1])

source. The quantum nature of an emitter can be demonstrated only by measuring temporal intensity correlations (or photon statistics) of the emitted light, i.e. the second-order auto-correlation function of the electric field, given by

$$g^{(2)}(\tau) = \frac{\langle E^{\dagger}(t)E^{\dagger}(t+\tau)E(t+\tau)E(t)\rangle}{\langle E^{\dagger}(t)E(t)\rangle^2} = \frac{\langle : I(t)I(t+\tau) : \rangle}{\langle I(t)\rangle^2} \tag{10.1}$$

where : : denotes normal ordering of the operators [4]. For totally uncorrelated light, as from a laser, $g^{(2)}(\tau) = 1$ for all $\tau$. However, for a number state $|n\rangle$, at $\tau = 0$ the second-order auto-correlation function drops to $g^{(2)}(0) = 1 - \frac{1}{n} < 1$ while for classical light sources $g^{(2)}(\tau) \geq 1$ for all $\tau$ [4]. Such a measurement of the $g^{(2)}$-function is used to prove non-classical light emission from single-photon sources.

For classical sources analysis of the photon statistics also provides useful information. For example, fluorescence correlation spectroscopy (FCS) [5–7] is widely used to characterize particle dynamics. In particular, diffusion coefficients, average concentrations, chemical reaction rates, molecular rotational Brownian motion, singlet-triplet dynamics, and spectral dynamics can all be observed using FCS [8–10].

When measuring the $g^{(2)}$-function with a single detector placed after the light source (Fig. 10.2a), photon arrival time differences $\tau$ shorter than the detector's dead time $t_d$ cannot be measured. Thus a measurement of the $g^{(2)}$-function can only be performed for time differences larger than the detector's dead time, any features for time differences $\tau < t_d$ cannot be resolved. This is crucial for the demonstration of non-classical light emission since here the task is to measure an antibunching feature at $\tau = 0$. If $t_d$ is of the same order or larger than the width of the antibunching dip, non-classical photon emission cannot be demonstrated with such a simple setup. This is the reason why the typical experimental setup for measuring the intensity auto-correlation function is the Hanbury-Brown and Twiss (HBT) setup [11], which is shown in Fig. 10.2b. In each of the outputs of a 50:50 beam splitter a detector is placed and time differences between clicks in detector start and detector stop are recorded. The $g^{(2)}$-function can be obtained from the distribution of these time differences for all photon arrival time differences $\tau$.

However, disadvantages of this configuration are the facts that the setup cannot be built as compactly as the one with a single detector and that more equipment is needed. Furthermore, for the setup with a single detector in principle one can obtain a higher count rate than for the one with a time difference measurement between a start and a stop detector. Last but not least, sometimes the HBT configuration gives rise to misleading interpretations of the experimental process. It may suggest that the photon has to "decide" at the beam splitter which way to take, rather than that the projection on one of the two possible paths is made when the photon is detected at either of the detectors.

Here, we present our experimental data for observing non-classical photon statistics with a single detector. As single-photon source we utilized a nitrogen vacancy (NV) centre in a diamond nanocrystal [3].

### *10.3.2 Experimental Results*

The lifetimes of NV centres in diamond nanocrystals are around 30 ns, which is very large compared to other single-photon sources as e.g. quantum dots. For resolving the interesting features of the corresponding $g^{(2)}$-function with a single detector that its dead time must be well below this value.

As a detector we utilized a fiber-coupled superconducting single-photon detector (SSPD). It consists of a 100 nm wide and 5 nm thick NbN meandering wire. This meander structure is fabricated on a sapphire crystal and covers an area of $10\,\mu\text{m} \times 10\,\mu\text{m}$ (Fig. 10.3a). The fabrication procedure is described elsewhere [12]. A fixed fiber-coupling to the detector area was implemented (Fig. 10.3b). For that purpose the sapphire was thinned to a thickness of $100\,\mu\text{m}$ and its back side was polished. The end facet of a single-mode fiber was aligned on the detector area and glued directly on the back side of the sapphire crystal. Figure 10.3d shows a scheme of the detector chip. For operation the detector was cooled to 4 K and biased at 90% of its critical current. Photon absorption in the detector causes a breakdown of the superconductance and thus a voltage pulse across the wire [12]. Figure 10.3c shows a scheme of the detector setup. The detector chip is mounted on a dip stick an immerged in liquid helium. These pulses from the detector are amplified by 76 dB at two 2 GHz bandwidth amplifiers. The inset in Fig. 10.4 shows a typical voltage curve for a photon absorption recorded with an oscilloscope of 2 GHz bandwidth. There was always a small reflection of the pulse observed after 14 ns which might be due to impedance mismatch. The dead time of the detector is $\leq$5 ns, the dark count rate is $<50\,\text{s}^{-1}$ and the quantum efficiency at 630 nm around 10%. The temporal resolution of the whole detector system was measured by applying femtosecond optical pulses from a titanium-sapphire laser. The voltage pulses of the SSPD and the trigger signal from the laser were connected to a time interval counter with 4 ps resolution. Such the time resolution of our system could be determined to 100 ps.

Figure 10.5 shows the experimental setup for measuring the $g^{(2)}$-function. Nanodiamonds were spin-coated on a coverslip and a single $NV^-$ centre was located

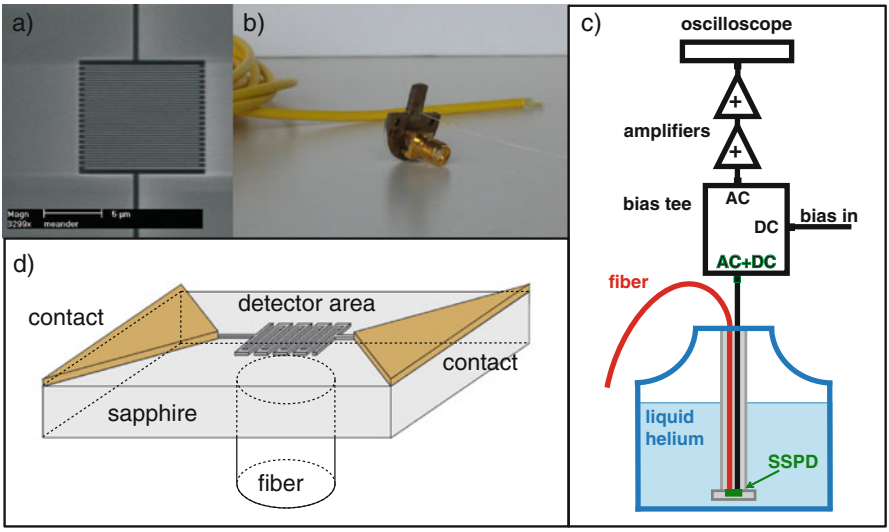


**Fig. 10.3** (**a**) STM picture of the detector area, which covers an area of $10\,\mu\text{m} \times 10\,\mu\text{m}$. (**b**) Fiber-coupled detector, mounted on a circuit board. (**c**) Detector System: The fiber-coupled chip is mounted on a dip-stick and immerged in liquid helium. It is connected to a bias-tee through which the bias current is provided. The short voltage pulses from the detector are amplified an fed to an oscilloscope. (**d**) Scheme of the fiber-coupled detector chip. (Reproduced from [1])

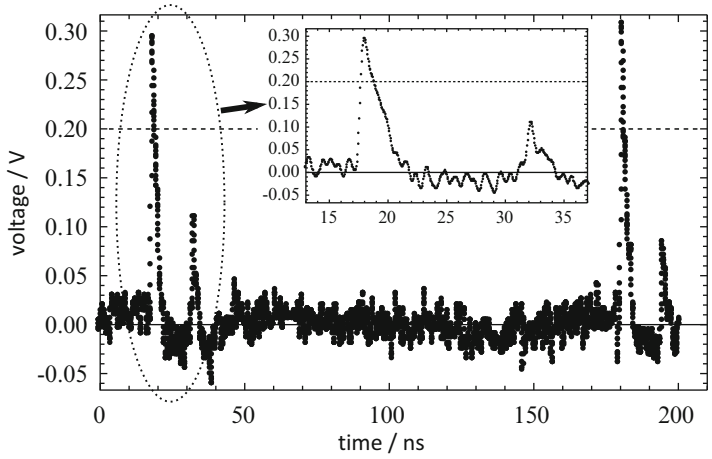


**Fig. 10.4** Typical trace with two detection events within a time window between 4 ns and 200 ns. The inset is a zoom of the first pulse

in a home-made inverted microscope as described elsewhere [13]. The excitation light was filtered out before the emission was coupled into a single mode optical fiber. Via the optical fiber the light was sent directly to the SSPD (Fig. 10.5a) or coupled to a standard free beam HBT-setup (Fig. 10.5b) with two avalanched

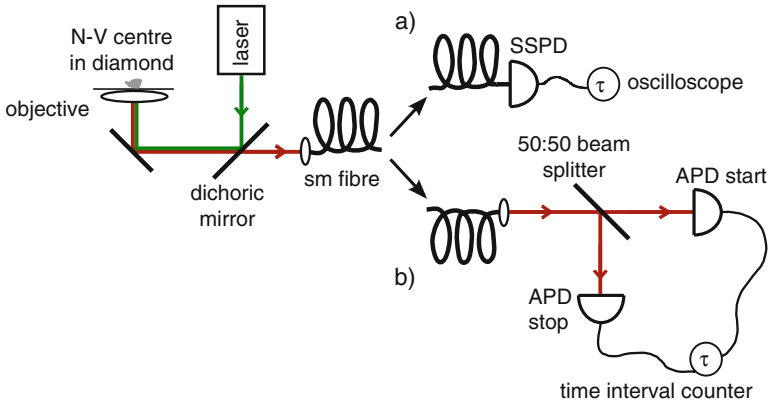


**Fig. 10.5** Experimental setup. Light from a single NV centre in a diamond nanocrystal is coupled to (**a**) a single fiber-coupled SSPD or (**b**) a free space HBT setup. (Reproduced from [1])

photodiodes (APDs) in the beam splitter outputs. In case (a) the voltage pulses from the SSPD were fed to an oscilloscope with 2 GHz bandwidth. The oscilloscope was programmed to save a pulse trace whenever a trigger level of 200 mV was exceeded twice with a time difference of between 4 ns and 200 ns. For this trigger level the reflections are neglected. A typical trace is shown in Fig. 10.4. For measuring the $g^{(2)}$-function, 30,000 traces were recorded and analysed. The distribution of the time differences between two trigger events was determined. In case (b) the time differences between signals from the APDs were recorded with a time interval counter.

The experimental results for the non-classical light source are shown in Fig. 10.6. For the same NV centre two different measurements were performed, one with a single SSPD and for comparison another one with a usual HBT setup with APDs in the beam splitter outputs. For the latter events from stray light due to the free beam operation were subtracted. The distributions of time differences for both experiments overlap very well. Single-photon statistics is clearly proven by both measurements. The black line is a fit to the APD measurement.

To summarize this section, we have shown experimentally that it is possible to prove non-classical light emission with only one detector. The required temporal resolution of the $g^{(2)}$-function was achieved because we utilized a superconducting single-photon detector with a short dead time compared to the lifetime of our single-photon source.

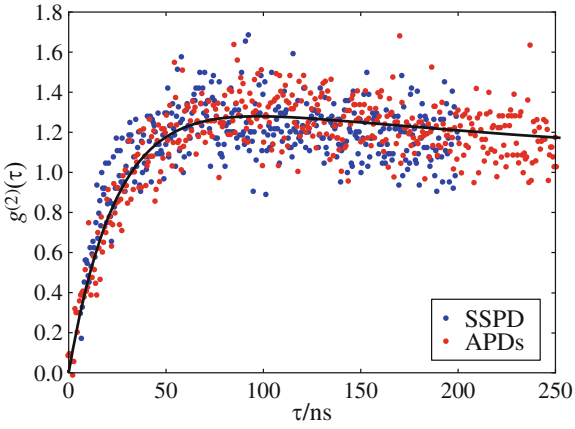


**Fig. 10.6** Measurement of the distribution of time differences between photon arrivals for a nonclassical light source (single NV centre), measured with a single detector (blue) and a HBT setup with two APDs (red). The black line is a fit to the data. (Reproduced from [1])

## 10.4 Application of a Room-Temperature Single Photon Source for Quantum Key Distribution (QKD)

The most promising candidates for practical true single photon sources (SPS) today are solid-state emitters, such as quantum dots (QDs) [14, 15] or defect centres in diamond [16, 17]. The latter have the tremendous advantage that they operate at room temperature and show now photo bleaching or blinking. This makes them ideal sources for non-classical light in a number of applications. For the nitrogen vacancy (NV) centre single photon rates exceeding 2 Mcps [18] were reported under continuous laser excitation. Other, presumably Cr-related centres with potentially even higher count rates have been investigated [19, 20], but their reliable fabrication is problematic and a full understanding of their structural properties is missing. Here we concentrate on the use of NV centres as SPS in quantum key distribution (QKD) [21, 22].

In QKD, high key rate and/or long distance experiments have been successfully implemented without true single photons using weak coherent laser pulses (WCP) [23, 24] together with the decoy state protocol [25, 26]. Although this protocol is secure against photon number splitting (PNS) attacks, it has the disadvantage of producing some overhead, because one explicitly uses vacuum and very low intensity pulses together with the signal pulses and also operates with faint pulses with a mean photon number per pulse of around 0.5. In addition, long-range QKD requires quantum repeaters where sources of single indistinguishable photons are advantageous over photon pair sources [27]. A true single photon source with high efficiency could therefore still be favourable in quantum information processing compared to WCP. Efficiency means that it emits a single photon into a well defined spectral and spatial mode with a probability near unity each time a trigger is applied. A practical SPS should also have a stable emission rate, be easy-to-use, should operate at room temperature and at high repetition frequencies.

In order to evaluate the applicability of the NV centre as reliable source for quantum information processing, in particular for QKD, it is desirable to use testbeds that allow for long-term measurements, implementation of different protocols, as well as straightforward integration of different defect centres. In this section, we report the realization of such a testbed. It consists of a short free-space transmission line combined with a compact SPS based on defect centres. The source relies on a specialized confocal setup for stable optical excitation and efficient collection of single photons from defect centres. Furthermore, it is designed in a way that it is easy to replace one kind of defect centre by another.

### *10.4.1 Compact and Versatile Design of a Single Photon Source Based on Defect Centres in Diamond*

The design of the source relies on a compact, portable and ready to use confocal setup. A $ZrO_2$ solid immersion lens (SIL) can be utilized to enhance the collection of single photons emitted from defect centres in nanodiamonds spin-coated directly on the SILs. Details of the fabrication of SILs with NV centres are provided in [18]. The source is built for single photon emitters with a wavelength range from 600 to 800 nm. With this it allows for the implementation of SPS using NV, SiV as well as Cr-based defect centres. Figure 10.7 shows a schematic (a) and a photograph (b) of the source which fits completely on an aluminum plate and has dimensions of only 22.5 cm $\times$ 19 cm $\times$ 9 cm. In this way the SPS is mobile and can easily be integrated in different experimental setups. The setup is robust against mechanical vibrations and thermal drifts due to its small size and compact mounting of all optical components. The generated single photon beam can either be freespace or fiber coupled by removal/addition of a single mirror which is equipped with a magnetic base. The sample unit holding the defect centres can either be the SIL with spin-coated defect centres or another substrate due to a removable sample holder. The setup is equipped with broadband optics and thus suitable for various defect centres, provided their emission wavelength is in the range of 600–800 nm. Only the exchangeable dichroic mirror has to be adapted together with the suitable excitation source. The sample holder is mounted on a 3-axes piezo stage. In order to keep track of the absolute position of the stage, sensors capable of detecting changes on a nanometer scale are used (SmarAct System). With this system it is possible to focus on a well defined position on the sample with very high accuracy and stability.

In principle, any kind of colour centre can be employed in the source described.

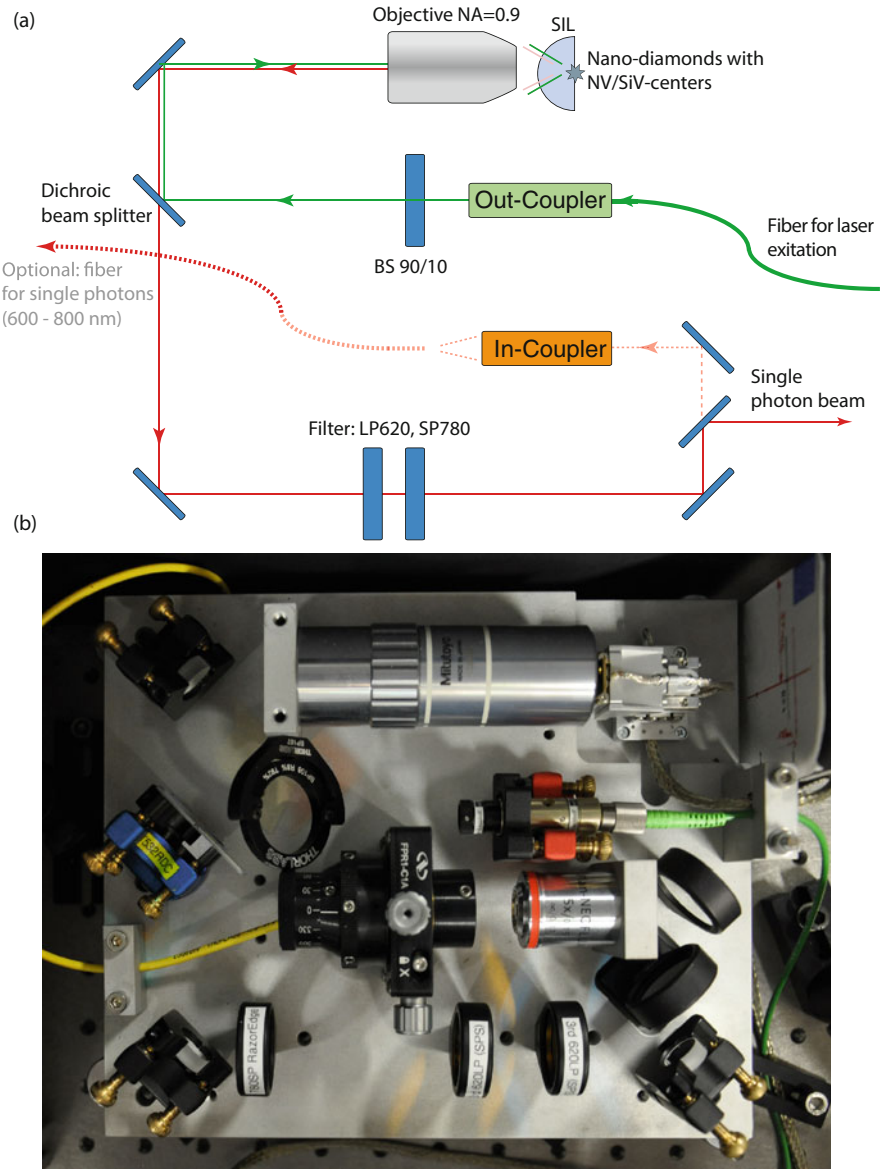


**Fig. 10.7** (**a**) Scheme and (**b**) photo of the compact confocal setup. The excitation laser is focused with a high NA objective onto the sample which is either one of several diamonds spincoated on a solid immersion lens (SIL) or grown on a substrat. The emission is collected by the same objective and then filtered by a dichroic beam splitter (exchangeable) and longpass (LP) and shortpass (SP) filters to clean it from residual laser light or fluorescence of the SIL or the substrate. (Reproduced from [2])

### 10.4.2 Properties of the NV Centre for QKD Applications

The quality of single photon emission, in particular the contribution of multi-photon events is routinely determined by measuring the second order autocorrelation function ($g^{(2)}(\tau)$) in a Hanbury-Brown Twiss (HBT) setup [11]. Although in the ideal case $g^{(2)}(\tau = 0) = 0$, a value of $g^{(2)}(\tau = 0) < 0.5$ is generally accepted as a criterion for single photon emission. Values below 0.12 have been reported with NV defect centres [18]. In QKD it is favourable to have photons at a well defined instant of time, thus pulsed excitation of the defect centres is of interest. In such a pulsed excitation scheme, using a green diode laser (PicoQuant LDH-P-FA-530 [28], 531 nm, pulse width <100 ps), we achieved count rates of 8900 cps at an excitation rate of 1 MHz for an NV centre in a nanodiamond which was spincoated on a SIL. This corresponds to an overall photon yield of 0.89% and a source efficiency of 2.9%. The latter is defined as the ratio of excitation pulses resulting in a single photon without background in the desired optical mode, here the freespace beam of the QKD experiment. This value is determined for a given overall photon yield by taking the overall transmission $\eta_{setup}$ of 0.31 of our setup, including the efficiency of ∼65% of the avalanche photodetectors (APDs), into account. For the QKD experiment, the maximal excitation rate was limited to frequencies up to 1 MHz by the modulation rate of the electro optic modulators (EOMs) (see section Fig. 10.4.3). A $g^{(2)}(0)$ value under pulsed excitation of 0.09, clearly indicating high purity single photon emission, is measured (Fig. 10.8a) using high resolution time-correlation electronics (PicoHarp 300 from PicoQuant). A lifetime of $28.5 \pm 1.5$ ns is calculated from the pulse shape.

### 10.4.3 Setup of QKD Testbed

The setup is shown in Fig. 10.9. The emitted freespace photons from the SPS are initially prepared in a linear polarization state by passing through a linear polarization filter after a $\lambda/2$ plate which is adjusted to maximize the count rate. After passing through a pinhole for further spatial mode cleaning, the photons impinge on the first EOM which is controlled by Alice. The EOM acts as a $\lambda/2$ and $\lambda/4$ plate, respectively, depending on the applied voltage. In this way two orthogonal linearly polarized photon states as well as two orthogonal circular polarization states can be encoded on the incoming photons, compliant to the BB84 protocol [29]. After passing through a lens system for recollimation, the photons pass through a second EOM, which is controlled by Bob. Bob randomly chooses a measurement basis by setting the voltage such that the EOM either does not modify the photons or acts as a $\lambda/4$ plate. A circular polarization is thus transformed into a linear one or vice versa. The linear polarization state can then be deterministically analyzed in a system consisting of a polarizing beam splitter (PBS), a linear polarization filter, compensating the non-perfect contrast of the PBS in reflection, and two avalanche

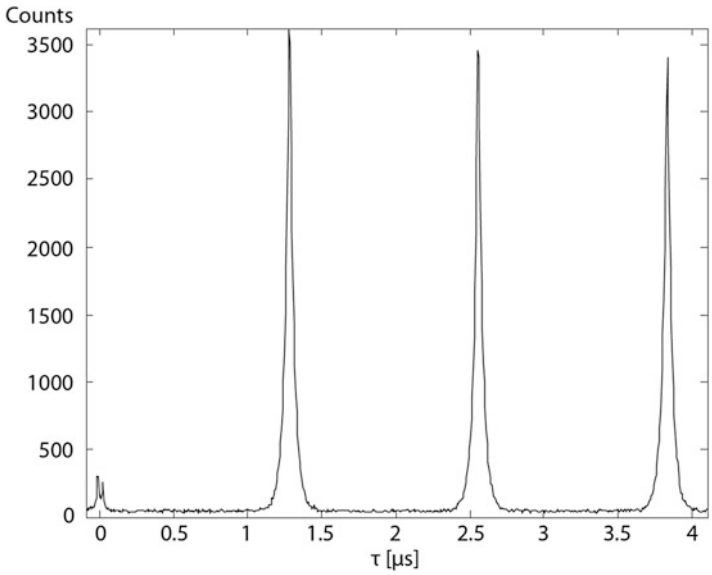


**Fig. 10.8** Measured intensities as a function of time for NV centre emission under pulsed excitation to calculate $g^{(2)}(\tau)$. The excitation rates were 800 kHz. The missing pulse at $\tau = 0$ indicates single photon emission. From the pulse shape we calculated al lifetime of the excited state of $28.5 \pm 1.5$ ns. (Reproduced from [2])

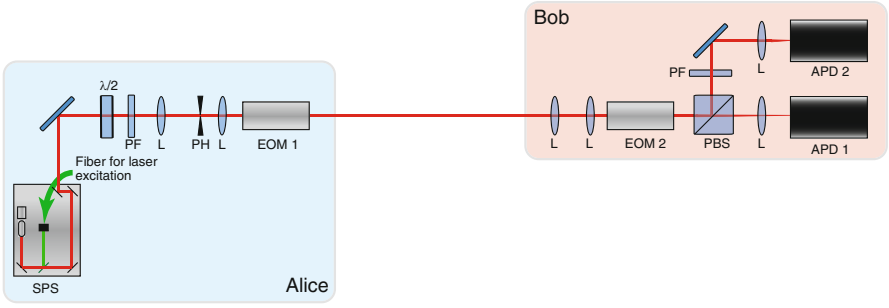


**Fig. 10.9** Schematics of the QKD testbed. Single photons are emitted from the source (SPS) and prepared in a well defined polarization state by the $\lambda/2$ plate and a polarization filter (PF). After collimation and spatial mode cleaning by two lenses (L) and a pinhole (PH), they pass through an electro-optical modulator (EOM 1). On Bob's side, the beam is recollimated by two lenses and then passes through a second modulator (EOM 2). Then, the polarization is analyzed by a polarizing beam splitter (PBS) and a polarization filter in the reflected mode of the PBS, which has a slightly reduced contrast compared to the transmitted mode. After passing through a lens for focusing, the photons are detected on one of two APDs. (Reproduced from [2])

**Table 10.1** Results of the QKD experiments in a test run for 300 s

| NV | |
|---|---|
| Repetition rate | 1 MHz |
| Count rate | $8.9 \pm 0.1$ kbit/s |
| Sifted keyrate | $3.99 \pm 0.05$ kbit/s |
| QBER | $3.0 \pm 0.2\%$ |
| Secured keyrate | 2.6 kbit/s |

photodiodes (APDs) (Perkin Elmer AQR). For the random bit and basis choice of Alice and Bob, quantum random numbers from the online random number service of HU Berlin and PicoQuant GmbH (http://qrng.physik.hu-berlin.de/), see also [30] are used.

The EOM is constructed in a way that it acts as a zero order waveplate. This minimizes its wavelength dependency during the modulation of different polarization states. However, especially when using the broadband NV centre as light source, possible dependencies between wavelength and transmitted polarization state could open the door to side-channel attacks which would have to be analyzed in way similar to the analysis of multiphotons (cf. Fig. 10.4.4 below, especially the notion of "tagged" photons).

### *10.4.4 Experimental Results*

In order to test the suitability of SPS based on the NV centre we ran the BB84 protocol in the QKD setup. The experimentally obtained parameters are summarized in Table 10.1. With the brightest NV centre, emitting at a count rate of 8.9 kcps, a sifted keyrate of 3.99 kbit/s at a quantum bit error rate (QBER) of 3% was achieved. The raw key was then further processed using the CASCADE protocol [31], resulting in a secure keyrate of 2.6 kbit/s. The CASCADE protocol is an efficient postprocessing protocol for the sifted key aiming at minimizing discrepancies between Alice and Bobs keys while at the same time minimizing Eves possible information about it. It consists of two steps: error correction by parity comparison between Alice and Bob and subsequent dilution of Eves information in the so-called privacy amplification. This privacy amplification is realized by a randomly chosen function belonging to a special class of hash functions. The observed QBER can be explained by the limited contrast of the polarization optics and the EOMs. The experiment ran with a stable emission rate over several hours, which was the necessary time to find the right EOM settings for transmission. This shows the long-term stability of our setup.

It is interesting to have a look at the source efficiencies and the $g^{(2)}(0)$ values of the SPS and their consequences on security concerning multiphoton events. An upper bound on the probability $p_{\mathrm{m}}$ to have multiphoton events in pulses emitted from a sub-Poisson light sources is given by [32],

$$p_{\mathrm{m}} \leq \frac{\mu^2 g^{(2)}(0)}{2}, \tag{10.2}$$

where $\mu$ is the mean photon number per pulse which is identical to the efficiency of the SPS to emit a single photon into the desired mode. This upper bound can then be used to calculate a lower bound on the secure keyrate $R$, which takes the unsecurity of having multiphoton events into account [33]:

$$R \geq q\{-Q_\mu f(E_\mu)H_2(E_\mu) + Q_\mu(1-\Delta)(1-H_2(E_\mu/(1-\Delta))\} \quad (10.3)$$

q is an efficiency factor depending on the exact protocol and expressing the randomness of the base choice, here it is 1/2, $Q_\mu$, the signal gain, is the fraction of detection events at Bob's side which is related to the signal with mean photon number $\mu$ (For an exact definition of $Q_\mu$, see i.e. [26]), f is the error correction efficiency of the postprocessing protocol, $E_\mu$ is the error rate of a signal with mean photon number $\mu$, and $H_2(x) = -x \cdot log_2(x) - (1-x) \cdot log_2(1-x)$ is the binary Shannon information function [34]. $\Delta$ is the ratio of "tagged" photons. "Tagged" photons are photon qubits emitted by a faulty source, wearing a "tag" with readable information for the eavesdropper revealing the actual basis of the qubit, cf. [33]. When more than one photon is emitted at a time, it carries the same information as its partner photon and can be regarded as a "tagged" photon when exploited by Eve in a PNS attack. For a single photon source $\Delta = p_\mathrm{m}/p_\mathrm{click}$, with the detection probability of a signal $p_\mathrm{click} \approx \mu \cdot \eta_\mathrm{total} + p_\mathrm{dc}$ [32]. $\eta_\mathrm{total}$ contains, besides the setup transmission $\eta_\mathrm{setup}$ (cf. Sect. 10.4.2), the transmission of the quantum channel. The darkcount probability $p_\mathrm{dc}$ is in our setup $2.4 \times 10^{-5}$.

Figure 10.10 shows the results of these secure keyrate calculations as a function of the channel loss. The secure key generation rate at 0 dB roughly reproduces our measured keyrate after postprocessing. For comparison we also plotted the secure

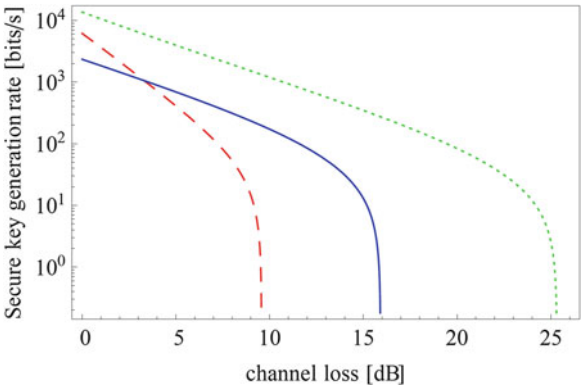


**Fig. 10.10** Secure key rates as a function of channel loss achieved with the BB84 protocol utilizing a true SPS with an NV centre. For comparison, the keyrate when using an attenuated laser without the decoy state protocol at the optimized mean photon number $\mu \sim \eta_{total}$, where $\eta_{total}$ is the overall transmission of the setup, is shown in red and dashed. Also shown in green and dotted is the secure keyrate when using WCP together with the decoy state protocol with a mean photon number of 0.5. (Calculated as in [36]; reproduced from [2])

keyrate of a potential experiment with identical parameters (please note that for lasers repetition rates might be chosen to be higher than particularly for the NV SPS), but with an attenuated laser instead of a single photon source with a mean photon number of $\mu \sim \eta_{\text{total}}$, which is approximately optimal for an attenuated laser without the decoy state protocol and when considering possible PNS attacks [35]. The keyrate is calculated as in Eq. 10.3, taking the multiphoton probability of a Poissonian lightsource into account. Also, the keyrate of an identical experiment with an attenuated laser source together with the decoy state protocol (the used mean photon number of 0.5 is calculated as in [36]) is shown. At low loss, attenuated laser pulses without the decoy state protocol have relatively high signal intensities and thus outperform our SPS, but at a certain channel loss (>3.3 dB) for the NV, cf. Fig. 10.10, translating into distances >8 km using a typical transmission of light through air in sea level of 0.4 dB/km the SPS provides higher secure keyrates and longer achievable transmission distances. This is due to a lower number of multiphoton events in a true SPS compared to an attenuated classical pulse of the same mean photon number. However, for the parameters achieved with single photon sources based on defect centres an attenuated laser together with the decoy state protocol is still favourable over our SPS regarding maximum keyrates and achievable distances. This is because the obtained efficiencies of the SPS is not high enough and at the same time the $g^{(2)}(0)$ value not low enough to outperform WCP together with the decoy state protocol (cf. Sect. 10.5). In this context, it is also interesting to note that even SPS sometimes have to be attenuated to reduce the small, but in a real source still existing fraction of multi-photon events to achieve the maximal possible transmission distance [32]. Even with high source efficiency, thus high mean photon number per excitation, security can be compromised at certain distances if the $g^{(2)}(0)$ value is not low enough. In fact for every $g^{(2)}(0)$ value and a given darkcount rate of the detectors, the maximal mean photon number to realize the longest distances can be estimated after the following formula, taken from [32]:

$$\mu_c = \sqrt{\frac{2p_{\text{dc}}}{g^{(2)}(0)}} \tag{10.4}$$

The ideal case would be to have a SPS which is above this critical mean photon number and to attenuate it in order to achieve the best rates at any distance. For our NV centre, we have an efficiency of 0.029 and a $g^{(2)}(0)$ of 0.09 (cf. Sect. 10.4.2). The critical mean photon number for this value of $g^{(2)}(0)$ is 0.039, a little above the given efficiency. There are examples of NV centres with higher efficiencies [18] which would surpass their critical mean photon number.

To summarize this section, single photon sources based on defect centres in diamond could outperform attenuated light sources in the future under optimistic but not unrealistic assumptions [2].

## 10.5 Conclusion

Defect centres in diamond have found many applications in the last years. On the one hand there are fundamental studies to learn about the quantum nature of electromagnetic field as we discussed in Sect. 10.3. More recently, we could also demonstrate the observation of the quantum Zeno effect using measurements on a single NV centre [37].

One the other hand, there are already true applications of single NV centers. In Sect. 10.4 we described a task in optical quantum technologies, i.e. quantum key distribution. Another direction is the use of NV centres in sensing. Aside from fundamental optical sensing, such as single emitter fluorescence lifetime imaging [38], there is by now a large activity on using NV centers as ulra-sensitive nanomagnetometer [39].

## References

1. Steudle G, Schietinger S, Höckel D, Dorenbos SN, Zadeh IE, Zwiller V, Benson O (2012) Measuring the quantum nature of light with a single source and a single detector. Phys Rev A 86:053814
2. Leifgen M, Schröder T, Gädeke F, Riemann R, Metillon V, Neu E, Hepp C, Arend C, Becher C, Lauritsen K, Benson O (2014) Evaluation of nitrogen- and silicon-vacancy defect centres as single photon sources in quantum key distribution. New J Phys 16:023021
3. Jelezko F, Wrachtrup J (2006) Single defect centres in diamond: a review. Phys Status Solidi A 203:3207–3225. https://doi.org/10.1002/pssa.200671403
4. Walls DF, Milburn GJ (2008) Quantum optics. Springer. https://doi.org/10.1007/978-3-540-28574-8
5. Magde D, Elson EL, Webb WW (1972) Thermodynamic fluctuations in a reacting system – measurement by fluorescence correlation spectroscopy. Phys Rev Lett 29:705–708. https://doi.org/10.1103/PhysRevLett.29.705
6. Elson EL, Magde D (1974) Fluorescence correlation spectroscopy. I. Conceptual basis and theory. Biopolymers 13:1–27. https://doi.org/10.1002/bip.1974.360130102
7. Magde D, Elson EL, Webb WW (1974) Fluorescence correlation spectroscopy. II. An experimental realization. Biopolymers 13:29–61. https://doi.org/10.1002/bip.1974.360130103
8. Schwille P (2001) Fluorescence correlation spectroscopy and its potential for intracellular applications. Cell Biochem Biophys 34:383–408. https://doi.org/10.1385/CBB:34:3:383
9. Webb WW (2001) Fluorescence correlation spectroscopy: inception, biophysical experimentations, and prospectus. Appl Opt 40:3969–3983. https://doi.org/10.1364/AO.40.003969
10. Marshall LF, Cui J, Brokmann X, Bawendi MG (2010) Extracting spectral dynamics from single chromophores in solution. Phys Rev Lett 105:053005. https://doi.org/10.1103/PhysRevLett.105.053005
11. Hanbury-Brown R, Twiss RQ (1956) Correlation between photons in two coherent beams of light. Nature 177:27–29. https://doi.org/10.1038/177027a0
12. Goltsman GN, Okunev O, Chulkova G, Lipatov A, Semenov A, Smirnov K, Voronov B, Dzardanov A, Williams C, Sobolewski R (2001) Picosecond superconducting single-photon optical detector. Appl Phys Lett 79:705. https://doi.org/10.1038/177027a0
13. Schietinger S, Barth M, Aichele T, Benson O (2009) Plasmon-enhanced single photon emission from a nanoassembled metal-diamond hybrid structure at room temperature. Nano Lett 9:1694–1698. https://doi.org/10.1021/nl900384c

14. Intallura PM, Ward MB, Karimov OZ, Yuan ZL, See P, Shields AJ, Atkinson P, Ritchie DA (2007) Quantum key distribution using a triggered quantum dot source emitting. Appl Phys Lett 91:161103. https://doi.org/10.1063/1.2799756
15. Heindel T, Kessler CA, Rau M, Schneider C, Fürst M, Hargart F, Schulz W-M, Eichfelder M, Rübach R, Nauerth S, Lermer M, Weier H, Jetter M, Kamp M, Reitzenstein S, Höfling S, Michler P, Weinfurter H, Forchel A (2012) Quantum key distribution using quantum dot single-photon emitting diodes in the red and near infrared spectral range. New J Phys 14:083001
16. Kurtsiefer C, Mayer S, Zarda P, Weinfurter H (2000) Stable solid-state source of single photons. Phys Rev Lett 85:290–293. https://doi.org/10.1103/PhysRevLett.85.290
17. Neu E, Steinmetz D, Riedrich-Möller J, Gsell S, Fischer M, Schreck M, Becher C (2011) Single photon emission from silicon-vacancy colour centres in chemical vapour deposition nano-diamonds on iridium. New J Phys 13:025012. https://doi.org/10.1088/1367-2630/13/2/025012
18. Schröder T, Gädeke F, Banholzer MJ, Benson O (2011) Ultrabright and efficient single-photon generation based on nitrogen-vacancy centres in nanodiamonds on a solid immersion lens. New J Phys 13:055017. https://doi.org/10.1088/1367-2630/13/5/055017
19. Aharonovich I, Castelletto S, Johnson BC, McCallum JC, Simpson DA, Greentree A, Prawer S (2010) Chromium single-photon emitters in diamond fabricated by ion implantation. Phys Rev B 81:121201. https://doi.org/10.1103/PhysRevB.81.121201
20. Aharonovich I, Castelletto S, Simpson DA, Greentree AD, Prawer S (2010) Photophysics of chromium-related diamond single-photon emitters. Phys Rev A 81:043813. https://doi.org/10.1103/PhysRevA.81.043813
21. Beveratos A, Brouri R, Gacoin T, Villing A, Poizat J-P, Grangier P (2002) Single photon quantum cryptography. Phys Rev Lett 89:187901. https://doi.org/10.1103/PhysRevLett.89.187901
22. Alléaume R, Treussart F, Messin G, Dumeige Y, Roch J-F, Beveratos A, Brouri-Tualle R, Poizat J-P, Grangier P (2004) Experimental open-air quantum key distribution with a single-photon source. New J Phys 6:92. https://doi.org/10.1088/1367-2630/6/1/092
23. Dixon AR, Yuan ZL, Dynes JF, Sharpe AW, Shields AJ (2010) Continuous operation of high bit rate quantum key distribution. Appl Phys Lett 96:161102. https://doi.org/10.1063/1.3385293
24. Schmitt-Manderbach T, Weier H, Fürst M, Ursin R, Tiefenbacher F, Scheidl T, Perdigues J, Sodnik Z, Kurtsiefer C, Rarity JG, Zeilinger A, Weinfurter H (2007) Experimental demonstration of free-space decoy-state quantum key distribution over 144 km. Phys Rev Lett 98. https://doi.org/10.1109/CLEOE-IQEC.2007.4386755
25. Hwang W-Y (2003) Quantum key distribution with high loss: toward global secure communication. Phys Rev Lett 91. https://doi.org/10.1103/PhysRevLett.91.057901
26. Lo H-K, Ma X, Chen K (2005) Decoy state quantum key distribution. Phys Rev Lett 94:230504. https://doi.org/10.1103/PhysRevLett.94.230504
27. Sangouard N, Simon C, Minar J, Zbinden H, de Riedmatten H, Gisin N (2007) Long-distance entanglement distribution with single-photon sources. Phys Rev A 76:050301. https://doi.org/10.1103/PhysRevA.76.050301
28. Schönau T, Riecke SM, Lauritsen K, Erdmann R (2011) Amplification of ps-pulses from freely triggerable gain-switched laser diodes at 1062 nm and second harmonic generation in periodically poled lithium niobate. Proc SPIE 7917:791707–791707. https://doi.org/10.1117/12.872114
29. Bennett CH, Brassard G (1984) Quantum cryptography: public key distribution and coin tossing. In: Proceedings of the IEEE international conference on computers, systems, and signal processing, Bangalore, vol 175. https://doi.org/10.1016/j.tcs.2014.05.025
30. Wahl M, Leifgen M, Berlin M, Röhlicke T, Rahn H-J, Benson O (2011) An ultrafast quantum random number generator with provably bounded output bias based on photon arrival time measurements. Appl Phys Lett 98:171105. https://doi.org/10.1063/1.3578456
31. Brassard G, Salvail L (1994) Secret-key reconciliation by public discussion. In: Helleseth T (ed) Advances in cryptology – EUROCRYPT 93, LNCS 765. Springer, Berlin/Heidelberg, pp 410–423. ISBN: 978-354057600-6

32. Waks E, Santori C, Yamamoto Y (2002) Security aspects of quantum key distribution with sub-Poisson light. Phys Rev A 66:042315. ISSN: 10502947
33. Gottesman D, Lo H-K, Lütkenhaus N, Preskill J (2004) Security of quantum key distribution with imperfect devices. Quantum Inf Comput 4:325–360. ISSN: 15337146
34. Shannon CE (1948) A mathematical theory of communication. Bell Syst Tech J 27:379–423, 623–656. https://doi.org/10.1002/j.1538-7305.1948.tb01338.x
35. Lütkenhaus N (2000) Security against individual attacks for realistic quantum key distribution. Phys Rev A 61:052304. ISSN:10502947
36. Ma X, Qi B, Zhao Y, Lo H-K (2005) Practical decoy state for quantum key distribution. Phys Rev A 72:012326. https://doi.org/10.1103/PhysRevA.72.012326
37. Wolters J, Strau M, Schoenfeld R-S, Benson O (2013) Quantum Zeno phenomenon on a single solid-state spin. Phys Rev A 88:020101. https://doi.org/10.1103/PhysRevA.88.020101
38. Schell AW, Engel P, Werra JFM, Wolff C, Busch K, Benson O (2014) Scanning single quantum emitter fluorescence lifetime imaging: quantitative analysis of the local density of photonic states. Nano Lett 14:2623–2627. https://doi.org/10.1021/nl500460c
39. Hong S, Grinolds MS, Pham LM, Le Sage D, Luan L, Walsworth RL, Yacoby A (2013) Nanoscale magnetometry with NV centers in diamond. MRS Bull 38:155–161. https://doi.org/10.1557/mrs.2013.23